

CONVERGENCE ANALYSIS OF THE INTRINSIC SURFACE FINITE ELEMENT METHOD

ELENA BACHINI¹ AND MARIO PUTTI²

ABSTRACT. The Intrinsic Surface Finite Element Method (ISFEM) was recently proposed to solve Partial Differential Equations (PDEs) on surfaces. ISFEM proceeds by writing the PDE with respect to a local coordinate system anchored to the surface and makes direct use of the resulting covariant basis. Starting from a shape-regular triangulation of the surface, existence of a local parametrization for each triangle is exploited to approximate relevant quantities on the local chart. Standard two-dimensional FEM techniques in combination with surface quadrature rules complete the ISFEM formulation thus achieving a method that is fully intrinsic to the surface and makes limited use of the surface embedding only for the definition of basis functions. However, theoretical properties have not yet been proved. In this work we complement the original derivation of ISFEM with its complete convergence theory and propose the analysis of the stability and error estimates by carefully tracking the role of the geometric quantities in the constants of the error inequalities. Numerical experiments are included to support the theoretical results.

Surface PDEs, Intrinsic Surface Finite Element Method, Convergence Theory
58J32, 65N30, 65N15

1. INTRODUCTION

Surface phenomena are ubiquitous in nature, playing an important role in mediating exchanges between contrasting media. They encompass a wide range of scales, from nano to planetary, with examples including earth processes [3, 8, 14–17], biological applications [22, 24, 26], and image processing [7, 29]. These models are typically based on partial differential equations (PDEs) governing balance laws of scalar, vector, and tensor quantities living on the surface. The detailed mathematical understanding of these PDEs is still limited, and applications are tackled by numerical techniques.

Most of the approaches developed so far for the discretization of surface PDEs rely heavily on the embedding in the ambient Euclidean space to project quantities back to the surface. In essence, the quantities of interest arising from the solution of the PDE are extended to a tubular neighborhood of the surface and then projected back to the surface or its piecewise interpolation, thus avoiding altogether the need to use charts [25]. This strategy has allowed the development of conforming and nonconforming finite element methods using the so-called Surface Finite Element (SFEM) originally developed in [12] (see [13] for a recent review), with extensions to discontinuous Galerkin [2] and low order virtual element methods [18]. A different approach has been recently proposed in [4], where the Intrinsic Surface Finite Element Method (ISFEM) has been developed and favorably compared to the embedded approach of [13] for the surface advection-diffusion-reaction equation, and to other available methods for the scalar and vector-valued surface heat equation [6]. A variant of ISFEM has been used to develop arbitrary order virtual elements on surfaces [5], by working directly on the chart, and thus needs a complete knowledge of the parametrization.

The ISFEM method is based on piecewise linear approximations of the discrete spaces and relies exclusively on geometric quantities that are intrinsic to the surface. The main advantage of ISFEM with respect to other embedded approaches is that the numerical solution, whether scalar, vector, or tensor, is an object intrinsically defined on the surface, avoiding the need to define its extension in \mathbb{R}^3 and its projection back to the surface. In addition, the ISFEM formulation in the scalar case requires only the knowledge of the tangent plane at the vertices of the surface triangulation in a form that can be exact, by means of the knowledge of the parametrization, or approximate, i.e., starting from point data. The embedding of the surface Γ in \mathbb{R}^3 is used exclusively in the definition of the basis functions, which are defined by lifting onto local tangent planes the first order polynomials defined either in the ambient space or on a local chart. As a consequence, the method can freely use different embeddings (metrics), can be adapted to multiple charts if available, and, unlike SFEM or other approaches (see e.g. [6, 25]), can be extended with few and straight-forward modifications to vector and tensor-valued PDEs (see [6] for the vector-valued case).

In this paper we develop the full numerical analysis of ISFEM, not yet addressed in previous work. It turns out that the convergence estimates arise directly from the redefinition of an appropriate scalar product intrinsic to Γ . We start with the identification of a proper Local Coordinate System (LCS) anchored on the surface Γ , we discuss the weak formulation of the PDE written in covariant form and defined on appropriate surface Sobolev spaces, e.g., $H^1(\Gamma)$ for a closed surface without boundary or $H_0^1(\Gamma)$ for a surface with homogeneous Dirichlet boundary. This operation introduces anisotropy due to the presence of the metric tensor arising from the first fundamental form of Γ . This anisotropy, whose ratio remains always bounded for a regular surface, adds to the eventual anisotropy of a tensor-valued diffusion coefficient. This added difficulty is counterbalanced by the fact that the ensuing numerical discretization, being defined on the LCS and thus on the chart or atlas, can exploit all the techniques developed for a planar two-dimensional domain and inherits all the related properties. For this reason, in our convergence estimates we discuss how the inequality constants depend upon the surface geometric quantities, intrinsic or extrinsic, i.e., depending on the first or second fundamental form. Our calculations show that optimal second order convergence is obtained under standard assumptions on the regularity of the mesh. This is experimentally discussed in the numerical results section, where convergence rates with respect to a manufactured solution are exposed and the behavior of the error constants at varying curvatures discussed. An example on a sphere defined by multiple charts is also presented.

2. THE INTRINSIC SURFACE FEM

Consider a compact surface $\Gamma \subset \mathbb{R}^3$ over which we would like to solve an elliptic equation of the form:

$$(1) \quad -\nabla_{\mathcal{G}} \cdot (\mathbb{D} \nabla_{\mathcal{G}} u) = f \quad \text{on } \Gamma,$$

where Γ is assumed to be fixed in time and the solution $u : \Gamma \rightarrow \mathbb{R}$ is a scalar function defined on the surface. The tensor \mathbb{D} is a rank-2 symmetric and positive-definite diffusion tensor, and we assume $f \in L^2(\Gamma)$. The differential operators $\nabla_{\mathcal{G}} \cdot$ and $\nabla_{\mathcal{G}}$, the surface divergence and gradient, respectively, need to be properly defined to follow the geometric setting of the problem. If the compact surface has no boundary, eq. (1) is augmented by the constraints of zero mean on u and f . If the surface has boundary (i.e., $\partial\Gamma \neq \{\emptyset\}$) we assume zero Neumann conditions, again implicitly augmented by the zero mean constraints, or zero Dirichlet boundary conditions. For the handling of non-homogeneous boundary conditions we refer to [9].

2.1. Geometrical setting. Let $\Gamma \subset \mathbb{R}^3$ be a 2-dimensional C^k regular surface. We recall that a surface $\Gamma \subset \mathbb{R}^3$ is said to be C^k regular if for any point $\mathbf{p} \in \Gamma$ there exists a map $\phi_{\mathbf{p}} : U \rightarrow \mathbb{R}^3$ of class C^k , with $U \subset \mathbb{R}^2$, such that $\phi_{\mathbf{p}}(U) \subset \Gamma$ is a neighborhood of \mathbf{p} , i.e., there exists an open neighborhood $V \subset \mathbb{R}^3$ of \mathbf{p} for which $\phi_{\mathbf{p}}(U) = V \cap \Gamma$, and such that $\phi_{\mathbf{p}}$ is a diffeomorphism of its image. The map $\phi_{\mathbf{p}}$ is called a local parametrization centered in \mathbf{p} . The inverse of the parametrization, $\phi_{\mathbf{p}}^{-1} : V \cap \Gamma \rightarrow U$, is called a local chart in \mathbf{p} . Explicitly, we have the following transformations:

$$\begin{aligned} \phi_{\mathbf{p}} : U &\longrightarrow V \cap \Gamma & \phi_{\mathbf{p}}^{-1} : V \cap \Gamma &\longrightarrow U \\ \hat{\mathbf{x}} &\longmapsto \mathbf{x} & \mathbf{x} &\longmapsto \hat{\mathbf{x}} \end{aligned}$$

where $\hat{\mathbf{x}} = (\hat{x}^1, \hat{x}^2)$ are the local coordinates, $\phi_{\mathbf{p}}(U)$ is the coordinate neighborhood, and $\mathbf{x} = (x^1, x^2, x^3)$ are the global Cartesian coordinates of a point on the surface. Given two points $\mathbf{p}, \mathbf{q} \in \Gamma$ and their local parametrizations $\phi_{\mathbf{p}}, \phi_{\mathbf{q}}$, with $U_{\mathbf{p}} \cap U_{\mathbf{q}} \neq \emptyset$, we say that the local parametrizations are compatible if the transition map $\phi_{\mathbf{p}} \circ \phi_{\mathbf{q}}^{-1}$ is a C^k diffeomorphism. We assume to have a family $\mathcal{A} = \{\phi_{\alpha}\}$ of compatible local parameterizations $\phi_{\alpha} : U_{\alpha} \rightarrow \Gamma$ such that $\Gamma = \cup_{\alpha} \phi_{\alpha}(U_{\alpha})$ (an atlas for Γ).

Given a point $\mathbf{p} \in \Gamma$, the practical construction of the relevant objects proceeds as follows [3, 4]. We calculate the two tangent vectors $\hat{\mathbf{t}}_1(\mathbf{p})$ and $\hat{\mathbf{t}}_2(\mathbf{p})$ on $T_{\mathbf{p}}\Gamma$:

$$\hat{\mathbf{t}}_i(\mathbf{p}) = d\phi_{\mathbf{p}}(\mathbf{e}_j(\mathbf{p})) = \left(\frac{\partial x^1}{\partial \hat{x}^i}, \frac{\partial x^2}{\partial \hat{x}^i}, \frac{\partial x^3}{\partial \hat{x}^i} \right), \quad i = 1, 2 \text{ and } j = 1, 2, 3,$$

where $d\phi_{\mathbf{p}}$ is the Jacobian matrix of the coordinate transformation and $\mathbf{e}_1(\mathbf{p}), \mathbf{e}_2(\mathbf{p}), \mathbf{e}_3(\mathbf{p})$ are the canonical basis vectors of \mathbb{R}^3 . For numerical stability, we orthogonalize via Gram-Schmidt the vector $\hat{\mathbf{t}}_2$ with respect to $\hat{\mathbf{t}}_1$, yielding the LCS orthogonal frame $\mathbf{t}_1, \mathbf{t}_2$ on $T_{\mathbf{p}}\Gamma$. We will denote by $\mathbf{s} = (s^1, s^2)$ the corresponding local coordinates. We denote with $\hat{\mathbf{J}}_{\mathbf{p}} = [\hat{\mathbf{t}}_1(\mathbf{p}), \hat{\mathbf{t}}_2(\mathbf{p})]$ the Jacobian matrix of the coordinate transformation between $\hat{\mathbf{x}}$ and \mathbf{x} , i.e., $d\phi_{\mathbf{p}}$, and collect the orthogonal reference vectors into the matrix $\mathbf{J}_{\mathbf{p}} = [\mathbf{t}_1(\mathbf{p}), \mathbf{t}_2(\mathbf{p})]$. Note that, $\mathbf{J}_{\mathbf{p}}$ is the Jacobian of the (unknown) coordinate transformation $\psi_{\mathbf{p}}$ between \mathbf{s} and \mathbf{x} , which exists due to the regularity of the surface. Given the above definitions, the unknown relation between the $\hat{\mathbf{x}}$ and \mathbf{s} coordinates can be formally written as $\mathbf{s} = \psi_{\mathbf{p}}^{-1} \circ \phi_{\mathbf{p}}(\hat{\mathbf{x}})$. On the other hand, its Jacobian is known explicitly and can be written as:

$$\mathbf{W}_{\mathbf{p}} := \mathbf{J}_{\mathbf{p}}^+ \hat{\mathbf{J}}_{\mathbf{p}} \in \mathbb{R}^{2 \times 2},$$

where $M^+ = (M^T M)^{-1} M^T$ is the pseudoinverse of the matrix $M \in \mathbb{R}^{3 \times 2}$.

Remark 2.1.1. Note that, $\mathbf{W}_{\mathbf{p}}$ is related to the Gram-Schmidt process that transforms the reference vectors $\{\hat{\mathbf{t}}_1(\mathbf{p}), \hat{\mathbf{t}}_2(\mathbf{p})\}$ into the orthogonal frame $\{\mathbf{t}_1(\mathbf{p}), \mathbf{t}_2(\mathbf{p})\}$.

In this setting, the metric tensor is diagonal and is given by:

$$(2) \quad \mathcal{G}(\mathbf{p}) := \begin{pmatrix} \|\mathbf{t}_1(\mathbf{p})\|^2 & 0 \\ 0 & \|\mathbf{t}_2(\mathbf{p})\|^2 \end{pmatrix} = \begin{pmatrix} g_{11}(\mathbf{p}) & 0 \\ 0 & g_{22}(\mathbf{p}) \end{pmatrix}.$$

The metric defines the surface scalar product $\langle \mathbf{u}, \mathbf{v} \rangle_{\mathcal{G}} = g_{ij} u^i v^j$, and has inverse denoted by $\mathcal{G}^{-1} = \{g^{ij}\}$. It is possible to show [11] that there exist constants $\mu_{*,\Gamma}$ and μ_{Γ}^* such that:

$$\mu_{*,\Gamma} \|\mathbf{v}\|^2 \leq \langle \mathbf{v}, \mathbf{v} \rangle_{\mathcal{G}} \leq \mu_{\Gamma}^* \|\mathbf{v}\|^2 \quad \text{for } \mathbf{v} \in T_{\mathbf{p}}\Gamma,$$

where $\mu_{*,\Gamma}, \mu_{\Gamma}^* \geq 1$ are the minimum and maximum eigenvalues of \mathcal{G} . Moreover, we have the following global uniform bounds on the norms and determinant of $\mathcal{G}(\Gamma)$:

$$(3) \quad c_{*,\Gamma} = \inf_{\mathbf{p} \in \Gamma} \|\mathcal{G}^{-1}(\mathbf{p})\|^2, \quad c_{\Gamma}^* = \sup_{\mathbf{p} \in \Gamma} \|\mathcal{G}^{-1}(\mathbf{p})\|^2, \quad g_{*,\Gamma} \leq \sqrt{\det(\overline{\mathcal{G}(\Gamma)})} \leq g_{\Gamma}^*.$$

We will be using the symbol $|\mathbb{I}_\Gamma|$ to denote the supremum over Γ of the norm of the second fundamental form. This value can be related to the curvatures of Γ .

Differential operators. Within this setting it is possible to define the relevant intrinsic differential operators. For the intrinsic gradient of a scalar function f we have $\nabla_{\mathcal{G}} f = \mathcal{G}^{-1} \nabla f$, where ∇f is the covariant derivative of f in the \mathbf{s} coordinates. We can write the intrinsic divergence of a (contravariant) vector $\mathbf{q} = q^1 \mathbf{t}_1 + q^2 \mathbf{t}_2$ as $\nabla_{\mathcal{G}} \cdot \mathbf{q} = \nabla \cdot \left(\sqrt{\det(\mathcal{G})} \mathbf{q} \right) / \sqrt{\det(\mathcal{G})}$. Note that here the flux vector $\mathbf{q} = -\mathbb{D} \nabla_{\mathcal{G}} f$ in eq. (1) is a vector tangent to Γ for a general (symmetric) diffusion tensor \mathbb{D} . Moreover, if $\mathbb{D} = \epsilon \mathbb{I}$, eq. (1) becomes the classical Laplace-Beltrami operator, i.e. $\nabla_{\mathcal{G}} \cdot (\mathbb{D} \nabla_{\mathcal{G}} f) = \epsilon \Delta_{\mathcal{G}} f$, where:

$$\Delta_{\mathcal{G}} f = \nabla_{\mathcal{G}} \cdot \nabla_{\mathcal{G}} f = \frac{1}{\sqrt{g_{11}g_{22}}} \left[\frac{\partial}{\partial s^1} \left(\sqrt{\frac{g_{22}}{g_{11}}} \frac{\partial f}{\partial s^1} \right) + \frac{\partial}{\partial s^2} \left(\sqrt{\frac{g_{11}}{g_{22}}} \frac{\partial f}{\partial s^2} \right) \right].$$

The standard tools deriving from Stokes theorems hold with the intrinsic operators without any modification. We first recall the formal definition of the integral of a function over a surface, which does not depend on the parametrization [1]:

Definition 2.1.2. *Let $f : \Gamma \rightarrow \mathbb{R}$ be a continuous function defined on a regular surface Γ with parametrization given by $\phi : U \rightarrow \Gamma$. The integral of f on Γ is:*

$$\int_{\Gamma} f = \int_{\phi^{-1}(\Gamma)} (f \circ \phi) \sqrt{\det(\mathcal{G})} \, ds.$$

Then, the following intrinsic Green's formula holds:

$$(4) \quad \int_{\Gamma} \langle \mathbb{D} \nabla_{\mathcal{G}} u, \nabla_{\mathcal{G}} v \rangle_{\mathcal{G}} = - \int_{\Gamma} \nabla_{\mathcal{G}} \cdot (\mathbb{D} \nabla_{\mathcal{G}} u) v + \int_{\partial\Gamma} \langle \mathbb{D} \nabla_{\mathcal{G}} u, \mu \rangle_{\mathcal{G}} v,$$

where $\mu : \Gamma \rightarrow \mathbb{R}^2$ denotes the vector tangent to Γ and normal to $\partial\Gamma$ with components written with respect to the curvilinear reference frame (i.e. $\mu = \mu^1 \mathbf{t}_1 + \mu^2 \mathbf{t}_2$).

2.2. Intrinsic variational formulation. Without loss of generality we assume that Γ is described by a single (global) parametrization $\phi : U \rightarrow \Gamma$. The ensuing results and the definitions extend directly to the case of a surface defined by an atlas assuming, as mentioned before, that the necessary transition maps are smooth.

Function spaces. We use standard definitions and notations for Sobolev spaces [11], which can be directly extended to a compact manifold Γ (see [20, 30]). We denote with $L^2(\Gamma)$ and $H^1(\Gamma)$ the classical Hilbert spaces on Γ . Explicitly:

$$L^2(\Gamma) = \left\{ v : \Gamma \rightarrow \mathbb{R} : \int_{\Gamma} v^2 < \infty \right\}, \quad H^1(\Gamma) = \left\{ v \in L^2(\Gamma) : \nabla_{\mathcal{G}} v \in (L^2(\Gamma))^2 \right\}.$$

Norms in $L^2(\Gamma)$ and $H^1(\Gamma)$ are denoted with $\|\cdot\|_{L^2(\Gamma)}$ and $\|\cdot\|_{H^1(\Gamma)}$, respectively, and are given by:

$$\|v\|_{L^2(\Gamma)}^2 = \int_{\Gamma} v^2 \quad \text{and} \quad \|v\|_{H^1(\Gamma)}^2 = \int_{\Gamma} v^2 + \int_{\Gamma} |\nabla_{\mathcal{G}} v|_{\mathcal{G}}^2,$$

where $|\nabla_{\mathcal{G}} v|_{\mathcal{G}}^2 = \langle \nabla_{\mathcal{G}} v, \nabla_{\mathcal{G}} v \rangle_{\mathcal{G}}$. We will also use the H^2 -seminorm given by:

$$|v|_{H^2(\Gamma)}^2 = \int_{\Gamma} |\nabla^2 v|_{\mathcal{G}}^2,$$

where $|\nabla^2 v|_{\mathcal{G}} = \text{tr}((\mathcal{G}^{-1} \nabla^2 v)^2)$ with $\nabla^2 v$ being the second covariant derivative of v . We note that:

$$\int_{\Gamma} |\nabla^2 v|_{\mathcal{G}}^2 \leq c_{\Gamma}^{*2} \left[\int_{\Gamma} |\partial^2 v|^2 + C_{\phi}^2 |\mathbb{I}_\Gamma|^2 \int_{\Gamma} |\partial v|^2 \right],$$

where C_ϕ is a generic constant depending on the parametrization, from which, recalling that $(\Delta_{\mathcal{G}}v)^2 = [\text{tr}(\mathcal{G}^{-1}\nabla^2v)]^2 \geq \text{tr}((\mathcal{G}^{-1}\nabla^2v)^2)$, it is easy to prove that the following holds:

$$(5) \quad c \|\partial^2 v\|_{L^2}^2 \leq |v|_{H^2}^2 \leq C \|\Delta_{\mathcal{G}}v\|_{L^2}^2 .$$

Note that the above inequalities are written without reference to the domain as they can be set equally on the surface Γ or the chart $\phi^{-1}(\Gamma) = U$.

Intrinsic variational problem. Now we can write the intrinsic variational formulation of the elliptic equation (1) in the LCS as:

Problem 2.2.1. Find $u \in H^1(\Gamma)$, with $\bar{u} = 0$, such that:

$$a(u, v) = F(v) \quad \forall v \in H^1(\Gamma) ,$$

where the “stiffness” bilinear form and the “forcing” linear form are given by:

$$a(u, v) = \int_{\Gamma} \langle \mathbb{D} \nabla_{\mathcal{G}} u, \nabla_{\mathcal{G}} v \rangle_{\mathcal{G}} \quad \text{and} \quad F(v) = \int_{\Gamma} f v .$$

Note that this is the direct extension to the surface Γ of the classical variational formulation of eq. (1). All the integrals are still written in intrinsic coordinates of our LCS.

Poincaré inequality. The dependence of the constants on the geometric characteristics of the surface originates mainly from the use of Poincaré inequality, which is given without proof in the following lemma.

Lemma 2.2.2. Let Γ a C^1 -regular surface without boundary and let $u \in H^1(\Gamma)$ be a function with average given by $\bar{u} = \frac{1}{|\Gamma|} \int_{\Gamma} u$. Then, there exists a constant $C_r > 0$ such that:

$$\|u - \bar{u}\|_{L^2(\Gamma)} \leq C_r \|\nabla_{\mathcal{G}} u\|_{L^2(\Gamma)} \quad \forall u \in H^1(\Gamma)$$

Poincaré inequality can be adapted to surfaces with Neumann or Dirichlet boundaries in the usual way (see, e.g., [9]). From now on we assume for simplicity that $\bar{u} = 0$. As a consequence, the L^2 the H^1 norms are equivalent, as stated in the next straight-forward corollary.

Corollary 2.2.3. Let Γ a C^1 -regular surface and let $u \in H^1(\Gamma)$ be a function with zero average, $\bar{u} = \frac{1}{|\Gamma|} \int_{\Gamma} u = 0$. Then, the following inequalities hold:

$$\|\nabla_{\mathcal{G}} u\|_{L^2(\Gamma)} \leq \|u\|_{H^1(\Gamma)} \leq \sqrt{1 + C_r^2} \|\nabla_{\mathcal{G}} u\|_{L^2(\Gamma)} .$$

Next we want to give detailed expressions of the constant C_r as a function of the geometric characteristics of Γ . We recall that the best Poincaré constant is related to the first nonzero eigenvalue of the Laplace-Beltrami operator on Γ . Indeed, it is easy to see that $C_r^2 = \lambda_1^{-1}$. Thus, we need to distinguish the three cases of a compact surface with no boundary, a surface with Dirichlet boundary $\partial\Gamma_D$ and a surface with Neumann boundary $\partial\Gamma_N$. Typically, bounds on these eigenvalues are given in terms of the Ricci curvature, but we note that for surfaces in \mathbb{R}^3 the Ricci and the Gaussian curvature coincide up to a positive multiplicative constant. For this reason we state everything in terms of the latter. We can summarize these results in the following lemma, whose proof can be found in [21].

Lemma 2.2.4. Let Γ be a regular surface with Gaussian curvature κ bounded from below by a constant $-R$ ($R > 0$), and denote by $\rho(\Gamma)$ the longest geodesic distance between two points. Then, there exist two positive constants C_1 and C_2 such that:

$$\lambda_1^N \geq \frac{C_1}{\rho(\Gamma)^2} \exp\left(-C_2 \rho(\Gamma) \sqrt{R}\right) , \quad \text{and} \quad \lambda_1^D \geq \frac{C_1}{\rho(\Gamma)^2} \exp\left(-C_2(1 + \rho(\Gamma) \sqrt{R})\right) ,$$

where λ_1^N identifies the case of a compact surface without boundary or with Neumann boundary and λ_1^D the case of Dirichlet boundary.

In what follows we will characterize all the constants in the ensuing inequalities by explicitly keeping track of C_Γ to quantify the geometrical effects of the properties of the surface domain on the error estimates.

Well-posedness. We list here the classical assumptions on the continuity and coercivity of the bilinear form and continuity of the linear form defining the weak formulation 2.2.1. For $a(\cdot, \cdot)$ we need the obvious hypothesis that the diffusion tensor \mathbb{D} be positive definite, i.e., there exist two positive constants d_* and d^* such that:

$$(6) \quad d_* \|\mathbf{v}\|_{\mathcal{G}}^2 \leq \langle \mathbb{D}\mathbf{v}, \mathbf{v} \rangle_{\mathcal{G}} \leq d^* \|\mathbf{v}\|_{\mathcal{G}}^2 \quad \text{for all } \mathbf{v} \in T_{\mathbf{p}}\Gamma \quad \text{and for all } \mathbf{p} \in \Gamma.$$

Then we can state the following lemma.

Lemma 2.2.5. *The bilinear form $a(\cdot, \cdot)$ in problem 2.2.1 is coercive and continuous, i.e., for any $u, v \in H^1(\Gamma)$ the following inequalities hold:*

$$(7) \quad a(u, u) \geq \frac{d_*}{1 + C_\Gamma^2} \|u\|_{H^1(\Gamma)}^2, \quad |a(u, v)| \leq d^* \|u\|_{H^1(\Gamma)} \|v\|_{H^1(\Gamma)}.$$

Moreover, the linear form $F(\cdot)$ is continuous:

$$F(v) \leq \|f\|_{L^2(\Gamma)} \|v\|_{L^2(\Gamma)}.$$

Proof. The proof is a standard application of the equivalence between the L^2 and H^1 norms in corollary 2.2.3 and the inequalities in eq. (6):

$$a(u, u) = \int_{\Gamma} \langle \mathbb{D} \nabla_{\mathcal{G}} u, \nabla_{\mathcal{G}} u \rangle_{\mathcal{G}} \geq d_* \|\nabla_{\mathcal{G}} u\|_{L^2(\Gamma)}^2 \geq \frac{d_*}{1 + C_\Gamma^2} \|u\|_{H^1(\Gamma)}^2.$$

For the continuity we write:

$$|a(u, v)| \leq \|\mathbb{D} \nabla_{\mathcal{G}} u\|_{L^2(\Gamma)} \|\nabla_{\mathcal{G}} v\|_{L^2(\Gamma)} \leq d^* \|u\|_{H^1(\Gamma)} \|v\|_{H^1(\Gamma)}.$$

The continuity of $F(\cdot)$ is simply an application of the Cauchy-Schwarz inequality. \square

Under the above assumptions, the Lax-Milgram theorem holds:

Lemma 2.2.6 (Lax-Milgram theorem). *Let $\mathcal{V}(\Gamma)$ be a Hilbert space and $a : \mathcal{V}(\Gamma) \times \mathcal{V}(\Gamma) \rightarrow \mathbb{R}$ be a continuous and coercive bilinear form. For all continuous linear forms $F : \mathcal{V}(\Gamma) \rightarrow \mathbb{R}$ there exists a unique function $u \in \mathcal{V}(\Gamma)$ such that:*

$$a(u, v) = F(v) \quad \forall v \in \mathcal{V}(\Gamma).$$

2.3. Intrinsic finite element method. We recall that our guiding principle that justifies certain choices is to maintain the scheme as intrinsic as possible, i.e., we want to use only intrinsic geometric quantities and minimize the use of the surface embedding.

The surface triangulation. Let $\mathcal{T}_h(\Gamma) = \cup_{i=1}^{N_T} T_i = \text{cl}(\Gamma)$ be a geodesic surface triangulation of Γ , formed by the union of non-intersecting surface triangles. We denote by Γ_h or $\mathcal{T}_h(\Gamma_h)$ the piecewise linear interpolation of Γ , i.e., the union of 2-simplices in \mathbb{R}^3 having the same vertices of $\mathcal{T}_h(\Gamma)$ and characterized by the mesh parameter h , the length of the longest chord between two triangle vertices in $\mathcal{T}_h(\Gamma)$. We assume that $\mathcal{T}_h(\Gamma_h)$ is shape-regular, i.e., there exists a constant $c > 0$ independent of h such that $r_T/h_T \geq c$ for all $T_h \in \mathcal{T}_h(\Gamma_h)$, where r_T is the radius of the circle inscribed in T_h and h_T is the longest side of T_h . By assumption, $\mathcal{T}_h(\Gamma_h)$ is a closely inscribed triangulation in the sense of [23], or equivalently, in the sense of [13], which means that $\mathcal{T}_h(\Gamma_h) \subset \mathcal{N}_\delta$, where \mathcal{N}_δ is

a tubular neighborhood of Γ of radius δ such that every point $\mathbf{p} \in \mathcal{N}_\delta$ has a unique orthogonal projection onto Γ . As a consequence, for every flat cell $T_h \subset \Gamma_h$ there corresponds a unique curved cell $T \subset \Gamma$, and this correspondence is bijective. Note that, the assumption of $\mathcal{T}_h(\Gamma)$ being geodesic is needed only to ensure the uniqueness of this correspondence. Finally, we introduce our working local chart $U_h \subset U$ and note that there exists an affine transformation \mathcal{F} such that $T_h = \mathcal{F}(U_h)$.

Intrinsic spatial discretization. Formally, we would like to work with the finite-dimensional \mathcal{P}_1 -conforming FEM space $\mathcal{V}_h(\mathcal{T}_h(\Gamma)) \subset H^1(\Gamma)$ given by:

$$(8) \quad \mathcal{V}_h(\mathcal{T}_h(\Gamma)) = \{v_h \in C^0(\mathcal{T}_h(\Gamma)) \text{ such that } v_h|_T \in \mathcal{P}_1(T) \quad \forall T \in \mathcal{T}_h(\Gamma)\}.$$

However, this definition is meaningless since we do not know how to define $\mathcal{P}_1(T)$, namely the space of first order polynomials in T . One way to circumvent this problem is proposed in [27, 28], where surface barycentric coordinates are used to generalize the classical linear interpolation on the surface. In this case the basis functions are nonlinear and their calculation requires the solution of local cell-wise quadratic minimization problems. Another approach is used in [5], where the equations, the variational formulation, and the VEM bilinear forms are defined on the chart. In this case, two-dimensional Lagrangian linear basis functions can be defined in the usual way directly on the chart and can be used to evaluate the needed integrals. This approach requires complete knowledge of the surface parametrization, since a triangulation of the chart is needed.

Maintaining the goal of ISFEM to make use of the surface embedding as little as possible, the following strategy for the definition of the basis functions can be devised. Working on an element-by-element basis as typical of FE methods, for each surface element T we consider the associated reference element $U_h = \phi_h^{-1}(T)$ eventually up to an affine transformation. Here, we require ϕ_h to be a Monge parametrization, i.e., $\phi_h = (\hat{x}^1, \hat{x}^2, \mathcal{H}(\hat{x}^1, \hat{x}^2))$, which always exists locally because Γ is regular. On U_h using the $\hat{\mathbf{x}}$ coordinates, we can define the standard local \mathcal{P}_1 basis functions $\hat{\varphi}_j^T(\hat{\mathbf{x}})$. By means of the composition with the local parametrization ϕ_h , we can formally define our local (nonlinear) basis function φ_j^T on T such that $\varphi_j^T(\mathbf{x}) := \hat{\varphi}_j^T \circ \phi_h^{-1}(\mathbf{x})$. Note that, on one hand we need to know the values of the basis functions and their derivatives only at the quadrature points $\mathbf{r}_i \in T$, on the other hand we want to use minimal information about the parametrization of the surface. In the case of \mathcal{P}_1 basis and trapezoidal quadrature rule, the quadrature points are the triangle vertices on both T and U_h , so that the basis function values are directly the nodal values $\varphi_j^T(\mathbf{p}_i) = \delta_{ij}$, $i, j = 1, 2, 3$. For the gradients, we need to perform a transformation to represent them in the orthogonal local reference frame $\{\mathbf{t}_1, \mathbf{t}_2\} \in T_{\mathbf{r}_i}T$ at each quadrature point. Practical computation of the surface gradient at the point \mathbf{r}_i yields:

$$(9) \quad \nabla_{\mathcal{G}} \varphi_j^T = \mathcal{G}_{\mathbf{r}_i}^{-1} \mathbf{J}_{\mathbf{r}_i}^+ \hat{\mathbf{J}}_{\mathbf{r}_i} \nabla \hat{\varphi}_j^T = \mathcal{G}_{\mathbf{r}_i}^{-1} \mathbf{W}_{\mathbf{r}_i} \nabla \hat{\varphi}_j^T.$$

Remark 2.3.1. *In case the height function \mathcal{H} is known, the Jacobian $\hat{\mathbf{J}}_{\mathbf{r}_i}$ takes on the following form:*

$$\hat{\mathbf{J}}_{\mathbf{r}_i} = [\hat{\mathbf{t}}_1(\mathbf{r}_i), \hat{\mathbf{t}}_2(\mathbf{r}_i)] = \begin{pmatrix} 1 & 0 \\ 0 & 1 \\ \frac{\partial \mathcal{H}}{\partial \hat{x}^1} & \frac{\partial \mathcal{H}}{\partial \hat{x}^2} \end{pmatrix},$$

while if \mathcal{H} is not known, we can recover $\hat{\mathbf{J}}_{\mathbf{r}_i}$ from the input tangent vectors by projection. The Jacobian $\mathbf{J}_{\mathbf{r}_i}$ is given by $\mathbf{J}_{\mathbf{r}_i} = [\mathbf{t}_1(\mathbf{r}_i), \mathbf{t}_2(\mathbf{r}_i)]$, with $\mathbf{t}_1, \mathbf{t}_2$ defined from $\hat{\mathbf{t}}_1, \hat{\mathbf{t}}_2$ by orthogonalization.

Remark 2.3.2. *We would like to stress here that $\nabla \hat{f}$ is the gradient of \hat{f} on the reference element calculated with respect to the $\hat{\mathbf{x}}$ coordinates. On the other hand, $\mathbf{W}_{\mathbf{r}_i} \nabla \hat{f}$ is the same gradient evaluated with respect to the \mathbf{s} coordinates, which may not be necessarily orthogonal in U_h but correspond to orthogonal reference vectors in $T_{\mathbf{r}_i}T$.*

Remark 2.3.3. *The ISFEM \mathcal{P}_1 basis functions described in [4] are equivalent to the ISFEM basis functions defined above. Indeed, if we consider T_h as our reference element U_h , then we can write $\tilde{\varphi}_j^T = \tilde{\varphi}_j^T \circ \mathcal{F}$ as a function in \mathbb{R}^3 . Moreover, ISFEM recovers the Surface FEM approach described in [13] if $T = T_h$.*

The last step in the definition of our global basis functions φ_k , $k = 1, \dots, N^{dof}$, is to glue together as usual the elemental components. Note that, because of tangent planes at vertices are defined uniquely, the resulting global basis functions are obviously conforming, albeit known only at the vertices. In conclusion, every function v_h in the functional space $\mathcal{V}_h(\mathcal{T}_h(\Gamma))$ can be written as:

$$(10) \quad v_h = I_h(v_h) = \sum_{k=1}^{N^{dof}} v_k \varphi_k,$$

where $I_h(v_h)$ indicates the ISFEM interpolant of v_h , and v_k are the nodal coefficients. Hence, the intrinsic FEM variational formulation can be written in the LCS as:

Problem 2.3.4. *Find $u_h \in \mathcal{V}_h(\mathcal{T}_h(\Gamma))$ such that*

$$a(u_h, v_h) = F(v_h) \quad \forall v_h \in \mathcal{V}_h(\mathcal{T}_h(\Gamma)),$$

where the linear and bilinear forms are given by:

$$a(u_h, v_h) = \int_{\Gamma} \langle \mathbb{D} \nabla_{\mathcal{G}} u_h, \nabla_{\mathcal{G}} v_h \rangle_{\mathcal{G}} \quad \text{and} \quad F(v_h) = \int_{\Gamma} f_h v_h.$$

Surface quadrature rules. Up to the definition of the ISFEM space $\mathcal{V}_h(\mathcal{T}_h(\Gamma))$, no numerical approximations are done until this point, since all the operators and integrals are defined on $\mathcal{T}_h(\Gamma)$ whose interior coincides with the surface Γ . We would like to remain within this setting as much as possible. Approximation issues arise when we need to practically compute quantities. To this aim, we assume that all the relevant geometric information related to the surface are known in exact or approximate (but consistent) form at the vertices of the triangulation and proceed by defining appropriate quadrature rules. In order to maintain optimal second order accuracy we need to provide quadrature rules whose error is locally proportional to h_T^2 . Thus we can consider surface extensions of the trapezoidal and the mid-point quadrature rules for triangles, as developed in [19], as modified and effectively used in [3, 4]. In this work we consider the trapezoidal rule given by:

$$(11) \quad \int_T f \approx Q_h(f) = \frac{1}{3} \sum_{j=1}^3 f(\mathbf{p}_j) \mathcal{A}_{T_h},$$

where \mathcal{A}_{T_h} is the cell area and $f(\mathbf{p}_j)$ are the evaluation of the function f at the cell nodes. We note that the above quadrature rule uses known information at the vertices of $\mathcal{T}_h(\Gamma)$, and thus does not require interpolation as the midpoint would.

Discrete norms. We will be using the discrete grid norm $\|f\|_h$ of a function $f \in \mathcal{V}_h(\mathcal{T}_h(\Gamma))$ defined as:

$$(12) \quad \|f\|_h^2 = \sum_{T \in \mathcal{T}_h(\Gamma)} \frac{\mathcal{A}_{T_h}}{3} \|f\|_{h,T}^2 = \sum_{T \in \mathcal{T}_h(\Gamma)} \frac{\mathcal{A}_{T_h}}{3} \sum_{j=1}^3 f(\mathbf{p}_j)^2 = \|f_h\|_h^2,$$

where $f_h = \{f_k\}_1^{N^{dof}} = \{f(\mathbf{p}_k)\}_1^{N^{dof}}$ is the vector of coefficients of the linear combination on the basis of $\mathcal{V}_h(\mathcal{T}_h(\Gamma))$. This norm is equivalent to the L^2 -norm and, as a consequence, to the H^1 -norm.

In fact, we can write:

$$\|f\|_{L^2(\Gamma)}^2 = \int_{\Gamma} f^2 = \sum_{T \in \mathcal{T}_h(\Gamma)} \int_T \left(\sum_{j=1}^3 f(\mathbf{p}_j) \varphi_j^T \right)^2 = \langle f_h, \mathbf{M} f_h \rangle,$$

The last scalar product can be controlled on both sides by the eigenvalues of the mass matrix \mathbf{M} to yield:

$$(13) \quad \frac{g^*}{4} \|f_h\|_h^2 \leq \|f\|_{L^2(\Gamma)}^2 \leq g^* \|f_h\|_h^2.$$

ISFEM formulation. Now all the ingredients of the ISFEM formulation are completed and we can write:

Problem 2.3.5 (ISFEM formulation). *Find $u_h \in \mathcal{V}_h(\mathcal{T}_h(\Gamma))$ such that*

$$a_h(u_h, v_h) = F_h(v_h) \quad \forall v_h \in \mathcal{V}_h(\mathcal{T}_h(\Gamma)),$$

where the linear and bilinear forms are given by:

$$a_h(u_h, v_h) = \sum_{T \in \mathcal{T}_h(\Gamma)} \frac{\mathcal{A}_{T_h}}{3} \sum_{j=1}^3 \langle \mathbb{D}(\mathbf{p}_j) \nabla_{\mathcal{G}} u_h(\mathbf{p}_j), \nabla_{\mathcal{G}} v_h(\mathbf{p}_j) \rangle_{\mathcal{G}},$$

and

$$F_h(v_h) = \sum_{T \in \mathcal{T}_h(\Gamma)} \frac{\mathcal{A}_{T_h}}{3} \sum_{j=1}^3 f_h(\mathbf{p}_j) v_h(\mathbf{p}_j).$$

3. NUMERICAL ANALYSIS OF ISFEM

In this section we provide H^1 estimates showing that the ISFEM achieves optimal convergence. The standard FEM theory is adapted to the intrinsic setting, with special attention to the analysis of the influence on convergence errors of surface geometric characteristics, such as, e.g., metric tensor and curvatures. For this purpose we will introduce in our analysis different constants. The symbol C will denote a generic constant not depending on h_T nor on surface properties. The symbol K_i will be used to identify constants that are independent of h_T but depend upon different surface geometric quantities. When working on single elements, we will use the symbol $K_{i,T}$ to denote the i -th constant defined on T .

As usual in FEM theory, this effort will be divided in two parts. First, the local analysis in section 3.1 will develop approximation and interpolation errors on a single triangle. Then, these local results will be combined in section 3.2 to yield the final estimates on the full surface.

3.1. Approximation errors on triangles. We start by summarizing some known results on approximation errors arising from the substitution of T with T_h [13, 23]. Then, interpolation and quadrature error estimates are addressed.

3.1.1. Surface approximation errors. Given a point $\mathbf{q} \in T_h$, we denote by $\text{pr}(\mathbf{q}) \in T$ the orthogonal projection of \mathbf{q} onto T along the direction $\mathbf{N}(\text{pr}(\mathbf{q}))$, normal to the surface in $\text{pr}(\mathbf{q})$. We state here some results related to the approximation of surface triangles, which can be easily extended to the entire surface. The proofs can be found in [13, lemma 4.1].

Lemma 3.1.1. *Given T_h , T and the projection map pr , the following estimates hold:*

- the distance between the approximate triangulation and the surface satisfies:

$$\max_{\mathbf{q} \in T_h} \left| \overrightarrow{\text{pr}(\mathbf{q})\mathbf{q}} \right| \leq Ch_T^2;$$

- the ratio δ_h between the area measures ds and dx of the surface triangle T and its approximation T_h , defined by $\text{ds} = \delta_h \text{dx}$, satisfies:

$$\|1 - \delta_h\|_{L^\infty} \leq Ch_T^2.$$

For any point $\mathbf{q} \in T_h$, we define the relative curvature of T_h with respect to Γ in \mathbf{q} as follows.

Definition 3.1.2. Given $K \subset T_h$, the relative curvature $\omega_\Gamma(\mathbf{q})$ of any point $\mathbf{q} \in K$ with respect to Γ is

$$\omega_\Gamma(\mathbf{q}) = \left| \overrightarrow{\text{pr}(\mathbf{q})\mathbf{q}} \right| |\Pi_{\text{pr}(\mathbf{q})}|.$$

Then, the relative curvature of K is $\omega_\Gamma(K) = \sup_{\mathbf{q} \in K} \omega_\Gamma(\mathbf{q})$.

With reference to [23], we can state the following surface approximation results.

Lemma 3.1.3. Given a geodesic triangulation $\mathcal{T}_h(\Gamma)$ with surface triangles T and geodesic edges σ , and their approximations T_h and σ_h in $\mathcal{T}_h(\Gamma_h)$, the following results hold.

- (1) The curvilinear length ℓ_σ of edge σ is related to the Euclidean length ℓ_{σ_h} of the chord σ_h via the inequalities:

$$\ell_{\sigma_h} \leq \ell_\sigma \leq \frac{1}{1 - \omega_\Gamma(\sigma_h)} \ell_{\sigma_h},$$

where $\omega_\Gamma(\sigma_h)$ is the relative curvature of σ_h with respect to Γ .

- (2) The difference between the unit vector $\mathbf{v}_{\overline{\mathbf{p}\mathbf{q}}}$ aligned to the chord σ_h and the unit tangent vector $\mathbf{t}_\mathbf{p}$ to the geodesic edge at \mathbf{p} satisfies:

$$\left| \mathbf{v}_{\overline{\mathbf{p}\mathbf{q}}} - \mathbf{t}_\mathbf{p} \right| \leq \frac{1}{2} |\Pi_T| \ell_\sigma.$$

- (3) The surface area of the cell T is related to the planar area of T_h by the relation:

$$|\mathcal{A}_T - \mathcal{A}_{T_h}| \leq C_T (\theta_{\max}^2 + \omega_\Gamma(T_h)),$$

where C_T is a constant depending on T and θ_{\max} is the maximum over all points $\mathbf{q} \in T_h$ of the angle between the tangent planes $T_\mathbf{q}T_h$ and $T_{\text{pr}(\mathbf{q})}T$.

The following lemma is a straight-forward consequence of the above results:

Lemma 3.1.4. For any $T_h \in \mathcal{T}_h(\Gamma_h)$ we have:

- the relative curvature can be bounded by:

$$\omega_\Gamma(T_h) = \sup_{\mathbf{q} \in T_h} \left| \overrightarrow{\text{pr}(\mathbf{q})\mathbf{q}} \right| |\Pi_{\text{pr}(\mathbf{q})}| \leq C |\Pi_T| h_T^2;$$

- the maximum angle between tangent planes of T and T_h can be bounded by:

$$\theta_{\max} \leq C |\Pi_T| h_T.$$

3.1.2. Interpolation and quadrature errors. We start with estimates of the interpolation errors in $\mathcal{V}_h(\mathcal{T}_h(\Gamma))$. We first note that that, using the metric bounds in eq. (3), it is easy to prove the following inequalities relating L^2 -norms of a function f and its gradient ∇f in the cell T and in

the chart U_h :

$$\begin{aligned} g_{*,T} \|f\|_{L^2(U_h)}^2 &\leq \|f\|_{L^2(T)}^2 = \int_T f^2 = \int_{U_h} f^2 \sqrt{\det(\mathcal{G})} \, ds \leq g_T^* \|f\|_{L^2(U_h)}^2, \\ g_{*,T} c_{*,T} \|\nabla f\|_{L^2(U_h)}^2 &\leq \|\nabla_{\mathcal{G}} f\|_{L^2(T)}^2 = \int_T |\nabla_{\mathcal{G}} f|^2 \\ &= \int_{U_h} |\mathcal{G}^{-1} \nabla f|^2 \sqrt{\det(\mathcal{G})} \, ds \leq g_T^* c_T^* \|\nabla f\|_{L^2(U_h)}^2. \end{aligned}$$

The following lemma provides the interpolation error estimate for $I_h(f)$ defined in eq. (10).

Lemma 3.1.5 (Interpolation error). *Given a function $f \in H^1(T)$, let $I_h(f)$ be the ISFEM interpolant in eq. (10). Then, we have:*

$$\|f - I_h(f)\|_{L^2(T)} \leq CK_{1,T} h_T^2 \|\partial^2 f\|_{L^2(U_h)},$$

$$\|\nabla_{\mathcal{G}} f - \nabla_{\mathcal{G}} I_h(f)\|_{L^2(T)} \leq CK_{2,T} h_T \|\partial^2 f\|_{L^2(U_h)},$$

where $K_{1,T} = \sqrt{g_T^*}$ and $K_{2,T} = \sqrt{c_T^* g_T^*}$.

Proof. Since $\mathcal{T}_h(\Gamma)$ is assumed to be shape-regular, using the standard planar interpolation error and definition of $I_h(f)$, we can write:

$$\|f - I_h(f)\|_{L^2(T)}^2 \leq g_T^* \|f \circ \phi_h - \pi_1(f)\|_{L^2(U_h)}^2 \leq C^2 g_T^* h_T^4 \|\partial^2 f\|_{L^2(U_h)}^2,$$

where $\pi_1(f)$ is the standard \mathcal{P}_1 interpolation of f in U_h . For the gradient we obtain:

$$\begin{aligned} \|\nabla_{\mathcal{G}} f - \nabla_{\mathcal{G}} I_h(f)\|_{L^2(T)}^2 &\leq c_T^* g_T^* \|\nabla(f \circ \phi_h) - \nabla \pi_1(f)\|_{L^2(U_h)}^2 \\ &\leq C^2 c_T^* g_T^* h_T^2 \|\partial^2 f\|_{L^2(U_h)}^2, \end{aligned}$$

where the gradient of the interpolant is intended in our *LCS*. \square

Next, we switch our attention to the accuracy of the surface quadrature rule. Following the results in [3] we show that the surface trapezoidal rule converges with optimal quadratic rate.

Lemma 3.1.6 (Surface Trapezoidal rule). *Given a function $f : T \rightarrow \mathbb{R}$, the surface trapezoidal rule is given by:*

$$Q_{h,T}(f) = \frac{A_{T_h}}{3} \sum_{j=1}^3 f(\mathbf{p}_j)$$

and satisfies:

$$\left| \int_T f - Q_{h,T}(f) \right| \leq Ch_T^2 \left(\|\partial^2 f\|_{L^2(U_h)} K_{1,T} + \|f\|_{h,T} K_{3,T} \right),$$

where $f(\mathbf{p}_i)$ is the value of f at the triangle vertices and $K_{3,T} = C_T |\mathbb{I}_T| (|\mathbb{I}_T| + 1)$.

Proof. We denote by $Q(f)$ the surface integral of the projection of f onto $\mathcal{V}_h(T)$, i.e., $Q(f) = \int_T I_h(f)$. Application of the triangular inequality to the quadrature error yields:

$$\left| \int_T f - Q_{h,T}(f) \right| \leq \left| \int_T f - Q(f) \right| + |Q(f) - Q_{h,T}(f)|.$$

From lemma 3.1.5 the first term can be bounded by:

$$\left| \int_T f - Q(f) \right| \leq Ch_T^2 \|\partial^2 f\|_{L^2(U_h)} K_{1,T},$$

while for the second term we use lemma 3.1.3, item 3:

$$\begin{aligned} |Q(f) - Q_{h,T}(f)| &\leq \frac{1}{3} \left| \sum_{j=1}^3 f(\mathbf{p}_j) \right| |\mathcal{A}_T - \mathcal{A}_{T_h}| \leq \frac{1}{3} \left(\sum_{j=1}^3 f(\mathbf{p}_j)^2 \right)^{1/2} |\mathcal{A}_T - \mathcal{A}_{T_h}| \\ &\leq \frac{1}{3} \|f\|_{h,T} C_T (\theta_{\max}^2 + \omega_\Gamma(T_h)) \leq \frac{1}{3} \|f\|_{h,T} C_T |\mathbb{I}_T| (|\mathbb{I}_T| + 1). \end{aligned}$$

Putting the two inequalities together we obtain:

$$\left| \int_T f - Q_{h,T}(f) \right| \leq Ch_T^2 \left(\|\partial^2 f\|_{L^2(U_h)} K_{1,T} + \|f\|_{h,T} C_T |\mathbb{I}_T| (|\mathbb{I}_T| + 1) \right).$$

□

As a remark, we note that, analogously, the midpoint rule is characterized by a similar error estimate, given by:

$$\left| \int_T f - Q_{h,M}(f) \right| \leq Ch_T^2 \left(\|\partial^2 f\|_{L^2(U_h)} K_{1,T} + \|f\|_{\infty,T} K_{3,T} \right),$$

where $f(\mathbf{m}_T)$ is the value of f at the centroid \mathbf{m}_T of T , having nodal coordinates given by $\mathbf{s}(\mathbf{m}_T) = \sum_{i=1}^3 \mathbf{s}(\mathbf{p}_i)/3$.

3.2. Convergence analysis. In this section we collect the previously developed local error estimates to build the global estimates forming the overall convergence theory of ISFEM. This analysis proceeds following a standard FEM approach by combining consistency with interpolation errors. Obviously, the developments must take into account the fact that our linear and bilinear ISFEM forms are approximated using the trapezoidal or the midpoint rule. This is handled in a usual fashion with the help of a discrete mesh norm $\|\cdot\|_h$, which is shown to be equivalent to the L^2 -norm on Γ to show coercivity of the discrete bilinear form. Then the surface extension of Strang lemma paves the way for the proofs of consistency and then of the final theorems on convergence in H^1 and L^2 norms. The latter, being exactly the surface extension of the Nitsche-Aubin duality trick, is only mentioned without proof. Everything will be done with the implicit assumption that the surface trapezoidal rule is employed. The results for the midpoint rule are exactly the same, and can be proved in a similar way.

We start our task by showing that the discrete bilinear form is coercive.

Lemma 3.2.1. *The discrete bilinear form $a_h(\cdot, \cdot)$ in problem 2.3.5 satisfies:*

$$a_h(v_h, v_h) \geq \frac{d_* \mu_{*,\Gamma}}{g_\Gamma^*(1 + C_\Gamma^2)} \|v_h\|_{H^1(\Gamma)}^2$$

Proof. Using Poincaré inequalities (corollary 2.2.3) and the equivalence between the discrete and L^2 -norms eq. (13), we obtain immediately:

$$\begin{aligned} a_h(v_h, v_h) &= \sum_{T \in \mathcal{T}_h(\Gamma)} \frac{\mathcal{A}_{T_h}}{3} \sum_{j=1}^3 \langle \mathbb{D}(\mathbf{p}_j) \nabla_{\mathcal{G}} v_h(\mathbf{p}_j), \nabla_{\mathcal{G}} v_h(\mathbf{p}_j) \rangle_{\mathcal{G}} \\ &\geq d_* \mu_{*,\Gamma} \|\nabla_{\mathcal{G}} v_h\|_h^2 \geq \frac{d_* \mu_{*,\Gamma}}{g_\Gamma^*(1 + C_\Gamma^2)} \|v_h\|_{H^1(\Gamma)}^2. \end{aligned}$$

□

The next step is the surface version of Strang lemma (see [10, Theorem 4.1.1] for the classical version of the proof):

Lemma 3.2.2 (Surface Strang-like lemma). *Let $u \in H^1(\Gamma)$ and $u_h \in \mathcal{V}_h(\mathcal{T}_h(\Gamma))$ be solutions of problem 2.2.1 and problem 2.3.5, respectively. Then, the error $u - u_h$ satisfies:*

$$\begin{aligned} \|u - u_h\|_{H^1(\Gamma)} \leq \inf_{v_h} \left[\left(1 + d^* \frac{g_\Gamma^*(1 + C_\Gamma^2)}{d_* \mu_{*,\Gamma}} \right) \|u - v_h\|_{H^1(\Gamma)} \right. \\ \left. + \frac{g_\Gamma^*(1 + C_\Gamma^2)}{d_* \mu_{*,\Gamma}} \sup_{w_h} \frac{|a(v_h, w_h) - a_h(v_h, w_h)|}{\|w_h\|_{H^1(\Gamma)}} \right] \\ + \frac{g_\Gamma^*(1 + C_\Gamma^2)}{d_* \mu_{*,\Gamma}} \sup_{w_h} \frac{|F(w_h) - F_h(w_h)|}{\|w_h\|_{H^1(\Gamma)}}. \end{aligned}$$

Proof. From the continuity of $a(\cdot, \cdot)$ (lemma 2.2.5) and the triangle inequality, we can write for all $v_h, w_h \in \mathcal{V}_h(\mathcal{T}_h(\Gamma))$:

$$\begin{aligned} |a_h(u_h - v_h, w_h)| &= |a(u - v_h, w_h) + a(v_h, w_h) - a_h(v_h, w_h) - F(w_h) + F_h(w_h)| \\ &\leq d^* \|u - v_h\|_{H^1(\Gamma)} \|w_h\|_{H^1(\Gamma)} + |a(v_h, w_h) - a_h(v_h, w_h)| + |F(w_h) - F_h(w_h)|. \end{aligned}$$

Using the coercivity of the discrete bilinear form, we obtain:

$$a_h(u_h - v_h, u_h - v_h) \geq \frac{d_* \mu_{*,\Gamma}}{g_\Gamma^*(1 + C_\Gamma^2)} \|u_h - v_h\|_{H^1(\Gamma)} \inf_{w_h} \|w_h\|_{H^1(\Gamma)},$$

or, equivalently:

$$\|u_h - v_h\|_{H^1(\Gamma)} \leq \frac{g_\Gamma^*(1 + C_\Gamma^2)}{d_* \mu_{*,\Gamma}} \sup_{w_h} \frac{|a_h(u_h - v_h, w_h)|}{\|w_h\|_{H^1(\Gamma)}}.$$

Putting together the two inequalities we obtain:

$$\begin{aligned} \|u - u_h\|_{H^1(\Gamma)} &\leq \|u - v_h\|_{H^1(\Gamma)} + \|u_h - v_h\|_{H^1(\Gamma)} \\ &\leq \|u - v_h\|_{H^1(\Gamma)} + \frac{g_\Gamma^*(1 + C_\Gamma^2)}{d_* \mu_{*,\Gamma}} \sup_{w_h} \frac{|a_h(u_h - v_h, w_h)|}{\|w_h\|_{H^1(\Gamma)}}, \end{aligned}$$

and taking the infimum over $v_h \in \mathcal{V}_h(\mathcal{T}_h(\Gamma))$, the result follows. \square

Note that the combination of the estimates of the interpolation error (lemma 3.1.5) and the trapezoidal rule error (lemma 3.1.6) shows that the scheme converges with optimal (first) order of accuracy in the $H^1(\Gamma)$ -norm. Indeed, it is possible to connect the constants of the error estimates with the geometric characteristics of Γ , as the following consistency lemma states.

Lemma 3.2.3 (Consistency). *For any continuous and coercive bilinear functional $a : \mathcal{V}(\Gamma) \times \mathcal{V}(\Gamma) \rightarrow \mathbb{R}$ and any continuous linear functional $F : \mathcal{V}(\Gamma) \rightarrow \mathbb{R}$ as given in problem 2.2.1, the discrete approximations $a_h : \mathcal{V}_h(\mathcal{T}_h(\Gamma)) \times \mathcal{V}_h(\mathcal{T}_h(\Gamma)) \rightarrow \mathbb{R}$ and $F_h : \mathcal{V}_h(\mathcal{T}_h(\Gamma)) \rightarrow \mathbb{R}$ given in problem 2.3.5 are consistent. In other words, we have that for, any $w_h \in \mathcal{V}_h(\mathcal{T}_h(\Gamma))$,:*

a) for the bilinear form $a(\cdot, \cdot)$:

$$(14) \quad |a(v_h, w_h) - a_h(v_h, w_h)| \leq$$

$$Ch^2 s \left(\frac{K_1}{g_{*,\Gamma} c_{*,\Gamma}} \|\partial^2 (\mathbf{W}^T \mathbb{D} \mathcal{G}^{-1} \mathbf{W})\|_{\infty, \Gamma} + K_3 \frac{2d^*}{\sqrt{g_{*,\Gamma}}} \right) \|v_h\|_{H^1(\Gamma)} \|w_h\|_{H^1(\Gamma)},$$

where $\|\partial^2 (\mathbf{W}^T \mathbb{D} \mathcal{G}^{-1} \mathbf{W})\|_{\infty, \Gamma}$ is the maximum over the element of the sup-norm of $\partial^2 (\mathbf{W}^T \mathbb{D} \mathcal{G}^{-1} \mathbf{W})$, and $K_i = \max_T K_{i,T}$, for $i = 1, 3$.

b) for the linear form $F_h(\cdot)$:

$$(15) \quad |F(w_h) - F_h(w_h)| \leq Ch^2 \left(\frac{K_1}{\sqrt{g_{*,\Gamma}}} \|\partial^2 f\|_{L^2(\Gamma)} + K_3 \|f\|_h \right) \|w_h\|_{H^1(\Gamma)}.$$

Proof. The proof is an application of lemma 3.1.6 to the special cases of integrands in the linear and bilinear forms. For the first part of the lemma eq. (14), we start by writing:

$$(16) \quad |a(v_h, w_h) - a_h(v_h, w_h)| \\ = \left| \int_{\Gamma} \langle \mathbb{D} \nabla_{\mathcal{G}} v_h, \nabla_{\mathcal{G}} w_h \rangle_{\mathcal{G}} - \sum_{T \in \mathcal{T}_h(\Gamma)} \frac{\mathcal{A}_{T_h}}{3} \sum_{j=1}^3 \langle \mathbb{D}(\mathbf{p}_j) \nabla_{\mathcal{G}} v_h(\mathbf{p}_j), \nabla_{\mathcal{G}} w_h(\mathbf{p}_j) \rangle_{\mathcal{G}} \right| \\ \leq \sum_{T \in \mathcal{T}_h(\Gamma)} \left| \int_T g - \frac{\mathcal{A}_{T_h}}{3} \sum_{j=1}^3 g(\mathbf{p}_j) \right| \\ \leq \sum_{T \in \mathcal{T}_h(\Gamma)} Ch_T^2 \left(\|\partial^2 g\|_{L^2(U_h)} K_{1,T} + \|g\|_{h,T} K_{3,T} \right)$$

where $g = \langle \mathbb{D} \nabla_{\mathcal{G}} v_h, \nabla_{\mathcal{G}} w_h \rangle_{\mathcal{G}}$. To estimate $\|\partial^2 g\|_{L^2(U_h)}$, we write g on the reference element U_h in the $\hat{\mathbf{x}}$ coordinate using eq. (9) obtaining $\langle \mathbb{D} \mathcal{G}^{-1} \mathbf{W} \nabla \hat{v}_h, \mathcal{G}^{-1} \mathbf{W} \nabla \hat{w}_h \rangle_{\mathcal{G}} = \langle \mathbf{W}^T \mathbb{D} \mathcal{G}^{-1} \mathbf{W} \nabla \hat{v}_h, \nabla \hat{w}_h \rangle$. Then, using standard two-dimensional arguments, we obtain the following inequality:

$$\|\partial^2 g\|_{L^2(U_h)} \leq \|\partial^2 (\mathbf{W}^T \mathbb{D} \mathcal{G}^{-1} \mathbf{W})\|_{\infty, T} \|\nabla \hat{v}_h\|_{L^2(U_h)} \|\nabla \hat{w}_h\|_{L^2(U_h)} \\ \leq \frac{1}{g_{*,T} c_{*,T}} \|\partial^2 (\mathbf{W}^T \mathbb{D} \mathcal{G}^{-1} \mathbf{W})\|_{\infty, T} \|\nabla v_h\|_{L^2(T)} \|\nabla w_h\|_{L^2(T)},$$

where we have used the fact that $\partial^2 \hat{v}_h = 0$ for \mathcal{P}_1 test functions. The final estimate is obtained by summation, where $\|\partial^2 (\mathbf{W}^T \mathbb{D} \mathcal{G}^{-1} \mathbf{W})\|_{\infty, \Gamma}$ is the maximum over all the elements of the sup-norm of $\partial^2 (\mathbf{W}^T \mathbb{D} \mathcal{G}^{-1} \mathbf{W})$. Recalling that $\|g\|_h = \|I_h(g)\|_h$, from continuity of the bilinear form and eq. (13), we obtain the following estimate directly written on Γ :

$$\|g\|_h^2 \leq \frac{4}{g_{*,\Gamma}} d^{*2} \|v_h\|_{H^1(\Gamma)}^2 \|w_h\|_{H^1(\Gamma)}^2.$$

Finally, we can put the previous inequalities together and sum over all the elements. The consistency estimate for the quadrature-based bilinear form then becomes:

$$|a(v_h, w_h) - a_h(v_h, w_h)| \\ \leq Ch^2 \left(\frac{K_1}{g_{*,\Gamma} c_{*,\Gamma}} \|\partial^2 (\mathbf{W}^T \mathbb{D} \mathcal{G}^{-1} \mathbf{W})\|_{\infty, \Gamma} + K_3 \frac{2d^*}{\sqrt{g_{*,\Gamma}}} \right) \|v_h\|_{H^1(\Gamma)} \|w_h\|_{H^1(\Gamma)},$$

where we set $K_i = \max_T K_{i,T}$, for $i = 1, 3$.

The proof of eq. (15) proceeds analogously with the definition of g replaced by $f w_h$. \square

The previous lemma together with the interpolation and quadrature errors yield the main convergence theorem for ISFEM.

Theorem 3.2.4 (Optimal H^1 -norm convergence). *The ISFEM approach converges in the H^1 -norm with optimal first order accuracy:*

$$\|u - u_h\|_{H^1(\Gamma)} \leq \mathbb{C}_1 h \|f\|_{L^2(\Gamma)} + \mathbb{C}_2 h^2 \|f\|_{H^2(\Gamma)}$$

where the constants $\mathbb{C}_1, \mathbb{C}_2$ depend on the surface Γ and its geometrical characteristics and on the upper and lower bounds of the diffusion tensor \mathbb{D} , but not upon the surface discretization.

Proof. The proof is a direct application of the previous two lemmas. Indeed, including the consistency estimates into the surface Strang-like lemma we obtain:

$$\begin{aligned} \|u - u_h\|_{H^1(\Gamma)} &\leq \inf_{v_h} \left[\left(1 + d^* \frac{g_\Gamma^*(1 + C_\Gamma^2)}{d_* \mu_{*,\Gamma}} \right) \|u - v_h\|_{H^1(\Gamma)} \right. \\ &\quad \left. + \frac{g_\Gamma^*(1 + C_\Gamma^2)}{d_* \mu_{*,\Gamma}} \sup_{w_h} \frac{|a(v_h, w_h) - a_h(v_h, w_h)|}{\|w_h\|_{H^1(\Gamma)}} \right] + \frac{g_\Gamma^*(1 + C_\Gamma^2)}{d_* \mu_{*,\Gamma}} \sup_{w_h} \frac{|F(w_h) - F_h(w_h)|}{\|w_h\|_{H^1(\Gamma)}} \\ &\leq C \left(1 + d^* \frac{g_\Gamma^*(1 + C_\Gamma^2)}{d_* \mu_{*,\Gamma}} \right) \frac{(K_2 + K_1 h)}{\sqrt{g_{*,\Gamma}}} h \|\partial^2 u\|_{L^2(\Gamma)} \\ &\quad + C \frac{g_\Gamma^*(1 + C_\Gamma^2)}{d_* \mu_{*,\Gamma}} h^2 \left[K_3 \left(\frac{2d^*}{\sqrt{g_{*,\Gamma}}} \|I_h(u)\|_{H^1(\Gamma)} + \|f\|_h \right) \right. \\ &\quad \left. + K_1 \left(\frac{1}{g_{*,\Gamma} C_{*,\Gamma}} \|\partial^2 (\mathbf{W}^T \mathbb{D} \mathcal{G}^{-1} \mathbf{W})\|_{\infty, \Gamma} \|I_h(u)\|_{H^1(\Gamma)} + \frac{\|\partial^2 f\|_{L^2(\Gamma)}}{\sqrt{g_{*,\Gamma}}} \right) \right], \end{aligned}$$

where we chose $v_h = I_h(u)$ and we used the inequality:

$$\begin{aligned} \|v_h\|_{H^1(\Gamma)}^2 &\leq \frac{g_\Gamma^*(1 + C_\Gamma^2)}{d_* \mu_{*,\Gamma}} a_h(v_h, v_h) \\ &= \frac{g_\Gamma^*(1 + C_\Gamma^2)}{d_* \mu_{*,\Gamma}} F_h(v_h) \leq \frac{g_\Gamma^*(1 + C_\Gamma^2)}{d_* \mu_{*,\Gamma}} \frac{4}{g_{*,\Gamma}} \|f_h\|_{L^2(\Gamma)} \|v_h\|_{L^2(\Gamma)}. \end{aligned}$$

Note that the last inequality comes directly from the continuity of $F_h(v_h)$. \square

The estimate in the above theorem contains on the right-hand-side a standard term related to the interpolation error plus a second term that goes to zero for a flat surface and it is thus compatible with standard FEM \mathcal{P}_1 estimates. Finally, we conclude this section by mentioning only that using the standard duality arguments optimal L^2 convergence is obtained.

4. NUMERICAL EXPERIMENTS

In this section we provide numerical support to the results presented in the previous sections. We present two different numerical experiments. In the first test case the aim is to show that the value of the constant in the L^2 -error for the solution and its gradient increases while the maximum value of the curvature increases. The second test case shows that the ISFEM method can be directly applied in the presence of multiple charts, if compatible sets of tangent vectors are available. Both test cases were considered already in [5] for the case of advection-diffusion-reaction equation discretized on the chart and numerically solved by means of a geometrically intrinsic version of the virtual element method. For the test case 2, we extend the result in [5] by directly solving the equation on the sphere, without the use of extra conditions at the interface of the two charts.

In all the experiments we consider a manufactured solution $u : \Gamma \rightarrow \mathbb{R}$ and calculate the resulting forcing function f by substitution into the original equation. Note that, even a simple manufactured solution would become highly nonlinear when considered on a surface, due to the spatially varying geometric information.

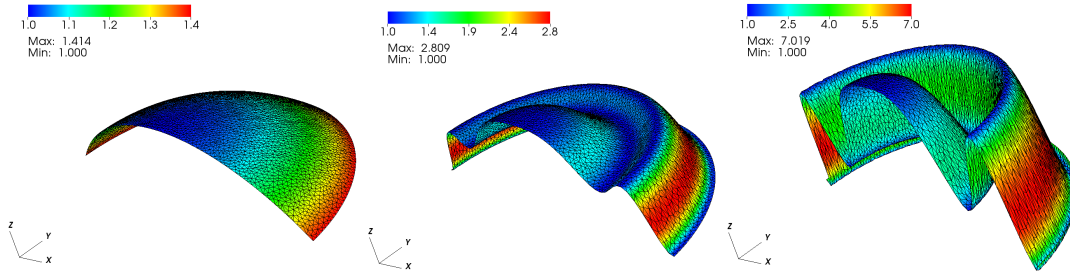


FIGURE 1. Surfaces described by eq. (17) with $r = 2$, $k = 5$ and $a = 0, 0.5, 2$, respectively in the left, middle and right panels. The color map shows the value of $\sqrt{\det(\mathcal{G}(\Gamma))}$.

Test case 1. For the test case 1 we consider the surface provided by the graph of the following height function (see [5]):

$$(17) \quad x^3 = \mathcal{H}(x^1, x^2) = \sqrt{r - (x^1)^2 - (x^2)^2 + a \cos^2 \left(k \frac{\pi}{2} ((x^1)^2 + (x^2)^2) \right)},$$

a trigonometric perturbation of a sphere, where r is the radius of the sphere, and a and k are the amplitude and the frequency of the cosine trigonometric perturbation. We use the Monge parametrization and define the surface by $\Gamma = \{(x^1, x^2, \mathcal{H}(x^1, x^2)) \mid x^2 \geq 0 \text{ and } (x^1)^2 + (x^2)^2 \leq 1\}$, with a radius $r = 2$ and a frequency $k = 5$. Figure 1 shows the surfaces obtained with different values of the amplitude a : a sphere ($a = 0$) is shown in the left panel, and two trigonometric deformations of the sphere are shown in the middle and left panels for the case $a = 0.5$ and $a = 2$, respectively. The color map shows the distribution in space of $\sqrt{\det(\mathcal{G}(\Gamma))}$. The mesh sets used in this test case are obtained from subsequent refinements of Delaunay triangulations of $U = \{(x^1, x^2) \mid x^2 \geq 0 \text{ and } (x^1)^2 + (x^2)^2 \leq 1\}$, then elevated using the height function eq. (17). We consider 8 levels of refinement, with a initial value of the surface mesh parameter $h \approx 0.25$ at $\ell = 0$. This corresponds to a total of 70 surface nodes for the case of $a = 0$ and $a = 0.05$, while for the case $a = 2$ the total number of nodes is 265 for $\ell = 0$. We define $u = x^1$ as manufactured solution and we compute an expression for the forcing function by the equation $f(s^1, s^2) = -\Delta_{\mathcal{G}} u$. We apply Dirichlet boundary condition by imposing the exact solution at the boundary nodes.

Figure 2 shows the L^2 -errors and experimental orders of convergence for the solution and its gradient. We notice second order convergence rates for the solution and first order for the gradient. Convergence rates slightly different than the optimal ones at the initial levels are attributable to a too coarse resolution of the surface triangulation, not accurate enough to approximate the surface. In particular, this phenomenon can be observed in the case of higher values of the parameter a that corresponds to higher values of the surface curvature.

Test case 2. We consider here $\Gamma = S^2$. We use two parametrizations, one for the northern and one for the southern hemispheres, to define two sets of tangent vectors and consider the equator as intersection set. A smooth transition map is known in this particular case. The stereographic projections for the northern hemisphere is given by:

$$(18) \quad \phi_N(s^1, s^2) = \left(\frac{2s^1}{1 + (s^1)^2 + (s^2)^2}, \frac{2s^2}{1 + (s^1)^2 + (s^2)^2}, \frac{1 - (s^1)^2 - (s^2)^2}{1 + (s^1)^2 + (s^2)^2} \right) = (x^1, x^2, x^3),$$

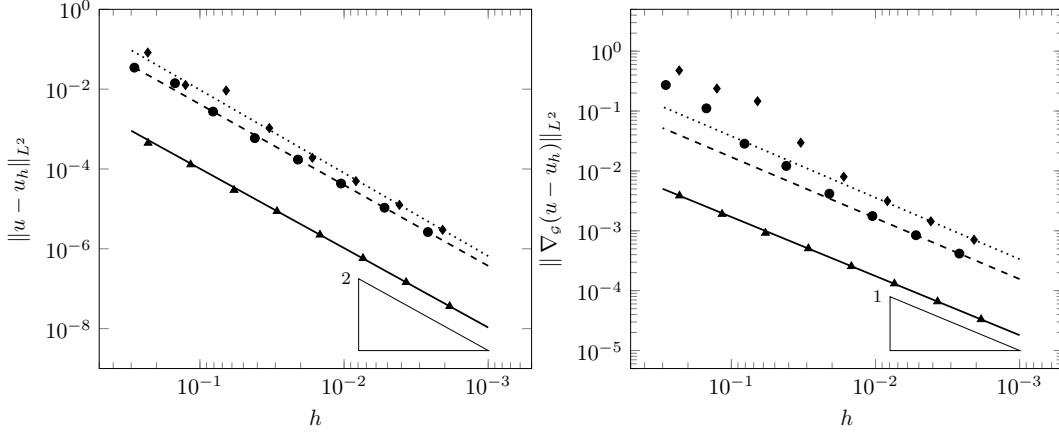


FIGURE 2. TC1: Numerical convergence of L^2 -errors for the solution (left) and its gradient (right) vs h on the surface triangulation. The convergence lines are obtained by means of least-square approximation considering the last 2 point values. The different lines denote the three different values of a considered: solid line with triangular data points is used for the case $a = 0$, dashed line with circular data points for $a = 0.5$, and dotted line with diamond data points for the case $a = 2$. The optimal theoretical slope is represented by the lower right triangles.

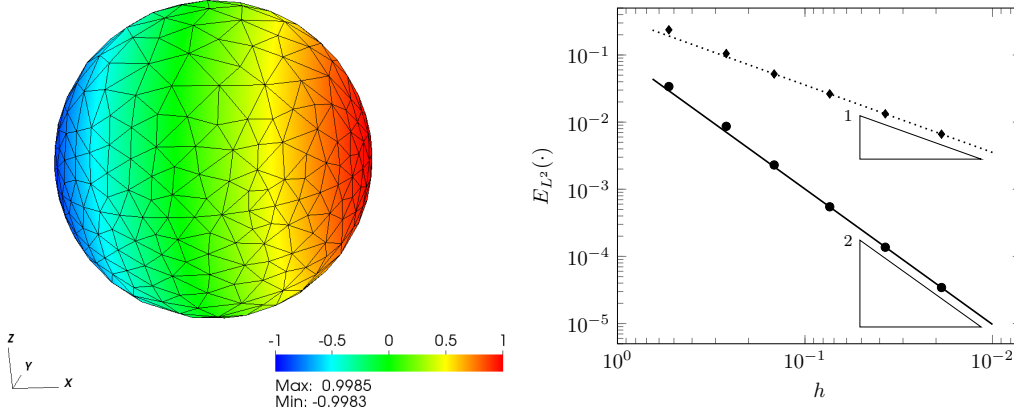


FIGURE 3. TC2: Numerical solution on the sphere (mesh level $\ell = 1$), left panel, and numerical convergences in the L^2 -norm for both the solution (solid line with circular data points) and its gradient (dotted line with diamond data points), right panel. The convergence lines are obtained by approximating via least-square the last 3 point values.

and similarly for the southern hemisphere, with the transition map between north and south written as:

$$\psi(s_N^1, s_N^2) = \left(\frac{s_N^1}{(s_N^1)^2 + (s_N^2)^2}, \frac{s_N^2}{(s_N^1)^2 + (s_N^2)^2} \right) = (s_S^1, s_S^2).$$

The surface triangulation of the sphere is obtained by computing a Delaunay triangulation of the disk, $U = \{(s^1, s^2) \mid (s^1)^2 + (s^2)^2 \leq 1\}$, then projecting the points to the surface using the two

stereographic projections. We consider a set of meshes with 6 levels of refinement, with a initial value of the surface mesh parameter $h = 0.532$ and a total of 111 surface nodes. Analogously to the first test case, we assume $u = x^1$ and compute the forcing function by $f(s^1, s^2) = -\Delta_g u + u$, where $x^1 \neq s^1$ because of the use of the stereographic projection. We note that, contrary to test case 1, we use the inverse of eq. (18) (as well as the south projection) to compute (s^1, s^2) from (x^1, x^2, x^3) in the evaluation of the forcing function. Figure 3 show on the left the manufactured solution and on the right the L^2 -errors and experimental orders of convergence for the solution and its gradient. Again, we notice an optimal order of convergence rates for both the solution and the gradient.

ACKNOWLEDGMENTS

This study received funding from the European Union - Next Generation EU National Recovery and Resilience Plan [NRRP], Mission 4, Component 2, Investment 1.3–D.D. 1243 2/082022, PE0000005 Extended Partnership “RETURN: Multi- Risk sciEnce for resilienT commUnities underR a changiNg climate” and Mission 4, Component 2, Investment 1.5 - Call for tender No. 3277 of 30 dicembre 2021 ECS00000043, No. 1058 of June 23, 2023, CUP C43C22000340006, “iN-EST: Interconnected Nord-Est Innovation Ecosystem”. The authors are members of the Gruppo Nazionale Calcolo Scientifico - Istituto Nazionale di Alta Matematica (GNCS-INdAM).

REFERENCES

- [1] M. Abate and F. Tovena. *Curves and Surfaces*. Springer-Verlag Italia, Milano, Italy, 2012.
- [2] P. F. Antonietti, A. Dedner, P. Madhavan, S. Stangalino, B. Stinner, and M. Verani. High order discontinuous Galerkin methods for elliptic problems on surfaces. *SIAM J. Num. Anal.*, 53(2):1145–1171, Jan. 2015.
- [3] E. Bachini and M. Putti. Geometrically intrinsic modeling of shallow water flows. *ESAIM Math. Model. Num. Anal.*, 54(6):2125–2157, 2020.
- [4] E. Bachini, M. W. Farthing, and M. Putti. Intrinsic finite element method for advection-diffusion-reaction equations on surfaces. *J. Comp. Phys.*, 424, 2021.
- [5] E. Bachini, G. Manzini, and M. Putti. Arbitrary-order intrinsic virtual element method for elliptic equations on surfaces. *Calcolo*, 58(30), 2021.
- [6] E. Bachini, P. Brandner, T. Jankuhn, M. Nestler, S. Praetorius, A. Reusken, and A. Voigt. Diffusion of tangential tensor fields: numerical issues and influence of geometric properties. *J. Numer. Math.*, 32(1):55–75, 2024. doi: doi:10.1515/jnma-2022-0088.
- [7] M. Bertalmio, L.-T. Cheng, S. Osher, and G. Sapiro. Variational problems and partial differential equations on implicit surfaces. *J. Comp. Phys.*, 174(2):759–780, Dec. 2001.
- [8] F. Bouchut and M. Westdickenberg. Gravity driven shallow water models for arbitrary topography. *Comm. Math. Sci.*, 2(3):359–389, Sept. 2004.
- [9] E. Burman, P. Hansbo, M. G. Larson, K. Larsson, and A. Massing. Finite element approximation of the Laplace–Beltrami operator on a surface with boundary. *Numer. Math.*, 141(1): 141–172, July 2018.
- [10] P. G. Ciarlet. *The finite element method for elliptic problems*. SIAM, 2002.
- [11] P. G. Ciarlet. *Linear and Nonlinear Functional Analysis with Applications*. SIAM, Oct. 2013.
- [12] G. Dziuk. Finite-elements for the Beltrami operator on arbitrary surfaces. *Lecture Notes in Mathematics*, 1357:142–155, 1988.
- [13] G. Dziuk and C. M. Elliott. Finite element methods for surfaces PDEs. *Acta Num.*, 22: 289–396, 2013.

- [14] I. Fent, M. Putti, C. Gregoretti, and S. Lanzoni. Modeling shallow water flows on general terrains. *Adv. Water Resour.*, 121:316–332, 2018.
- [15] E. D. Fernández-Nieto, F. Bouchut, D. Bresch, M. J. Castro Díaz, and A. Mangeney-Castelnau. A new Savage–Hutter type model for submarine avalanches and generated tsunami. *J. Comp. Phys.*, 227(16):7720–7754, Aug. 2008.
- [16] A. Ferroni, L. Formaggia, and A. Fumagalli. Numerical analysis of Darcy problem on surfaces. *ESAIM Math. Model. Num. Anal.*, 50(6):1615–1630, Oct. 2016.
- [17] N. Flyer, E. Lehto, S. Blaise, G. B. Wright, and A. St-Cyr. A guide to RBF-generated finite differences for nonlinear transport: Shallow water simulations on a sphere. *J. Comp. Phys.*, 231(11):7133–7151, June 2012.
- [18] M. Frittelli and I. Sgura. Virtual element method for the Laplace-Beltrami equation on surfaces. *ESAIM Math. Model. Num. Anal.*, 52(3):965–993, Sept. 2018.
- [19] K. Georg and J. Tausch. Some error estimates for the numerical approximation of surface integrals. *Math. Comp.*, 62(206):755–763, 1994.
- [20] E. Hebey. *Nonlinear Analysis on Manifolds: Sobolev Spaces and Inequalities: Sobolev Spaces and Inequalities*, volume 5. American Mathematical Soc., 2000.
- [21] P. Li. *Geometric Analysis*. Cambridge Studies in Advanced Mathematics. Cambridge University Press, 2012.
- [22] J. Lowengrub, J. Allard, and S. Aland. Numerical simulation of endocytosis: Viscous flow driven by membranes with non-uniformly distributed curvature-inducing molecules. *J. Comp. Phys.*, 309:112–128, 2016.
- [23] J.-M. Morvan. *Generalized Curvatures*, volume 2 of *Geometry and Computing*. Springer Science & Business Media, Berlin, Heidelberg, May 2008.
- [24] M. P. Neilson, J. A. Mackenzie, S. D. Webb, and R. H. Insall. Modeling cell movement and chemotaxis using pseudopod-based feedback. *SIAM J. Sci. Comput.*, 33(3):1035–1057, Jan. 2011.
- [25] M. Nestler, I. Nitschke, and A. Voigt. A finite element approach for vector- and tensor-valued surface pdes. *J. Comp. Phys.*, 389:48–61, 2019. ISSN 0021-9991.
- [26] I. Nitschke, A. Voigt, and J. Wensch. A finite element approach to incompressible two-phase flow on manifolds. *J. Fluid Mech.*, 708:418, 2012.
- [27] O. Sander. Geodesic finite elements for cosserat rods. *Int. J. Numer. Methods Engrg.*, 82(13):1645–1670, 2010.
- [28] O. Sander. Geodesic finite elements on simplicial grids. *Int. J. Numer. Methods Engrg.*, 92(12):999–1025, 2012.
- [29] C. Stöcker and A. Voigt. Geodesic evolution laws - A level-set approach. *SIAM J. Imag. Sci.*, 1(4):379–399, 2008.
- [30] M. E. Taylor. *Partial Differential Equations I: Basic Theory*. Applied Mathematical Sciences. Springer New York, 2010.

¹ DEPARTMENT OF MATHEMATICS “TULLIO LEVI-CIVITA”, UNIVERSITY OF PADUA, ITALY (ELENA.BACHINI@UNIPD.IT),

² DEPARTMENT OF AGRONOMY, FOOD, NATURAL RESOURCES, ANIMALS AND ENVIRONMENT, UNIVERSITY OF PADUA, ITALY (MARIO.PUTTI@UNIPD.IT)